Journal of Materials Chemistry A

ROYAL SOCIETY OF CHEMISTRY

COMMUNICATION

View Article Online
View Journal | View Issue

Cite this: J. Mater. Chem. A, 2024, 12, 1422

Received 9th June 2023
Accepted 9th December 2023

DOI: 10.1039/d3ta03423b

rsc.li/materials-a

Steric hindrance driven passivating cations for stable perovskite solar cells with an efficiency over 24%†

Kasparas Rakstys,‡*[a] Jianxing Xia,‡[b] Yi Zhang,[b] Kotryna Siksnelyte,[a] Andre Slonopas,[c] Paul J. Dyson,[b] Vytautas Getautis*[a] and Mohammad Khaja Nazeeruddin*[b]

In this work, a series of passivating salts for perovskite solar cells (PSCs) based on *ortho*-methylammonium iodide functional units are molecularly engineered to study the steric hindrance driven passivation effect. The incorporation of fluorine atoms into passivating agents has been found to be beneficial not only for maximized defect passivation effect, ensuring improved charge transport, but also for significantly enhanced hydrophobicity of the perovskite film, leading to enhanced device stability. The highest power conversion efficiency (PCE) of over 24% has been achieved for surficial passivated PSCs based on fluorinated cation **PFPDMAI$_2$**. Importantly, long-term operational stability over 1500 h is demonstrated showing the great prospect of a simple passivation strategy forming a thin organic halide salt layer instead of a 2D perovskite layer on the surface.

Perovskite solar cells (PSCs) because of their outstanding photovoltaic properties, simple and low-cost solution fabrication process, abundant precursors, and skyrocketing power conversion efficiency (PCE) have attracted tremendous attention all over the world and show great promise for scale-up and future commercialization.[1–9] While the unprecedentedly high efficiency using perovskites is an astonishing achievement, on the other hand, issues relating to the long-term durability against atmospheric moisture and oxygen, heat, and light still raise concern for successful commercial application of PSC technology.[10–14]

Compositional and dimensional engineering of perovskites, interface passivation, and charge transport layer optimization are proven to be effective pathways to improve the performance of PSCs.[15–21] However, disordered stoichiometric compositions at surfaces and the heterogeneous spontaneous polycrystalline perovskite formation inevitably generate abundant defects at surfaces and grain boundaries causing undesired charge recombination, limiting the further improvement of PCE due to significant loss of the open-circuit voltage (V_{oc}) and fill factor (FF). Moreover, the presence of defects causes stability issues due to the phase segregation during cell operation and induced ion migration at the perovskite/HTM interface.[22–26] Therefore, developing innovative solutions to passivate the perovskite defects is essential.

Until now, surficial passivation using alkylammonium halides has been traditionally employed to form an additional Ruddlesden–Popper or Dion–Jacobson two-dimensional (2D) perovskite phase on top of the 3D perovskite to improve the performance of perovskite devices.[27–34] However, a stubborn in-plane orientation and high exciton binding energy are identified as limiting factors of 2D perovskite layers, which suppress charge transport and draw back the passivation effect, especially under device operating conditions and when bulky spacer cations are used.[35–37] In this regard, we have recently studied the energy barrier of 2D perovskite formation using sterically hindered cations, which prevent the formation of surficial 2D perovskite layers at elevated temperatures and maximize the passivation effect on both shallow- and deep-level defects.[15] Moreover, the strongly interacting intramolecular systems effectively suppress the nonradiative recombination loss and improve the device performance. It is known that the introduction of a weak electron-accepting functionality (*i.e.* halo, carbonyl, sulfonyl) into the molecular structure enhances the dipole moment, being advantageous for intramolecular charge transfer.[38–41] On the other hand, it is known that the uncoordinated Pb^{2+} ions at the surface of the perovskite result in a defective perovskite layer, and also act as charge recombination centers hindering the charge transfer. In addition,

[a]*Department of Organic Chemistry, Kaunas University of Technology, Radvilenu pl. 19, Kaunas 50254, Lithuania. E-mail: kasparas.rakstys@ktu.lt; vytautas.getautis@ktu.lt*
[b]*Institute of Chemical Sciences and Engineering, École Polytechnique Fédérale de Lausanne, CH-1951 Sion, Switzerland. E-mail: mdkhaja.nazeeruddin@epfl.ch*
[c]*Johns Hopkins University, Whiting School of Engineering, Department of Materials Science and Engineering, USA*

† Electronic supplementary information (ESI) available: Detailed synthetic procedures, device fabrication and characterization, SEM and XRD data, detailed photovoltaic parameters along with *J–V* curves, fitting parameters of bi-exponential decay function in TRPL. See DOI: https://doi.org/10.1039/d3ta03423b

‡ K. R. and J. X. contributed equally.

molecules containing electron-accepting groups have been shown to interact with uncoordinated Pb^{2+}, passivating the defects of halide vacancies.[42–50]

In this work, we explore *ortho*-methylammonium substituted cations to reveal the steric hindrance driven passivation effect. Combining different structural units, four organic salts were designed and successfully synthesized employing facile chemistry using commercially available and cheap reagents. Employing novel surface passivating agents for the post-treatment of perovskite films suppresses nonradiative recombination and improves interfacial charge extraction, resulting in a PCE of over 24% in PSCs with enhanced long-term stability. With this, we demonstrate a simple defect passivation method that significantly improves perovskite solar cell efficiency and stability.

Organic passivation salts were designed and synthesized using straightforward procedures with high purity and excellent yields. In general, brominated substrates were converted to amine derivatives using Gabriel synthesis, followed by treatment with hydrogen iodide to yield ammonium iodides required for 3D perovskite passivation. As shown in Fig. 1, four different cations with tailored functional units were prepared based on *ortho*-phenylenedimethylammonium iodide **PDMAI$_2$**, 3,4-thiophenedimethylammonium iodide **TDMAI$_2$**, perfluoro-*ortho*-phenylenedimethylammonium iodide **PFPDMAI$_2$**, and 1,2,3,4,5,6-phenylenehexamethylammonium iodide **PHMAI$_6$**. The chemical structures of the synthesized compounds were verified by NMR spectroscopy, mass spectrometry, and elemental analysis. Detailed synthetic procedures and analysis are reported in the ESI.†

The density functional theory (DFT) was employed to study the interaction at the molecular and atomic scales, where the (001) perovskite surface with 2 × 2 periodicity in the *x*–*y* plane acts as the adsorption slab. The optimized geometries of passivating cations laying on the perovskite surface (Fig. 1) show that the NH_3^+ group of cations interacted with the surrounding iodine atoms. The cations **PFPDMAI$_2$** and **PHMAI$_6$** exhibit stronger surface iodine atom relaxation than that of **PDMAI$_2$** and **TDMAI$_2$**, indicating that the introduction of F atoms and increasing the number of NH_3^+ groups within the cations will enhance the surface interactions. Compared with **PDMAI$_2$**, **TDMAI$_2$** and **PFPDMAI$_2$**, the six NH_3^+ groups in **PHMAI$_6$** will change the stand of surface cations on the perovskite to lay on the PbI_2 terminal surface. The molecules having two ammonium groups are vertically interacted with the tetrahedron cage of the perovskite (001) surface, such as the **PDMAI$_2$**, **TDMAI$_2$**, **PFPDMAI$_2$**. The detailed difference is the tiny angular rotation between the molecules towards the perovskite surface.

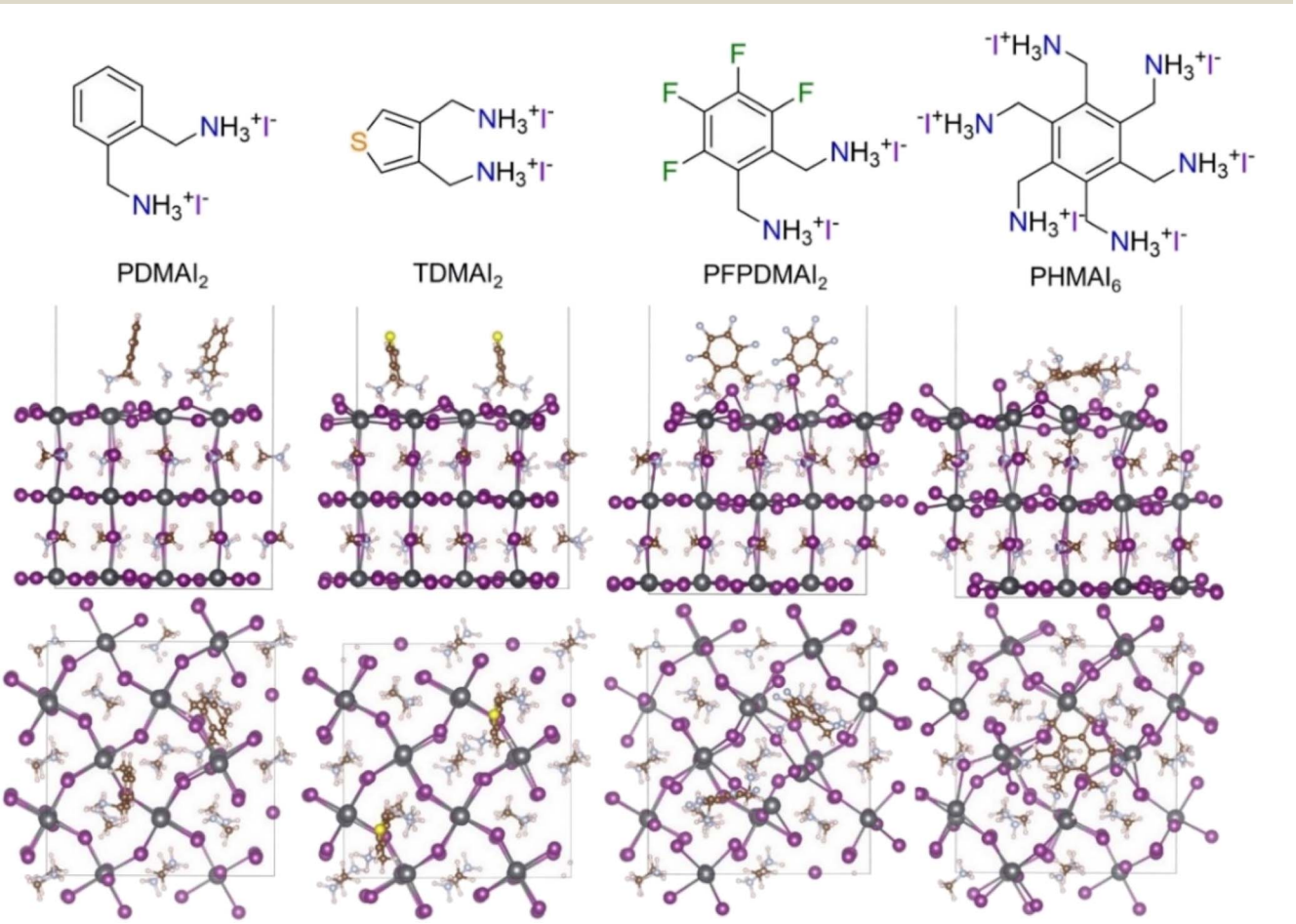

Fig. 1 The chemical structures and optimized geometries of synthesized passivating agents laying on the perovskite surface.

However, the **PHMAI$_6$** with six active ammonium groups lays on the perovskite tetrahedron cage *via* the benzene ring, because of the multiple interaction sites. The binding energy (E_b) of cations laying on the perovskite (001) surface was further employed to study the interfacial interaction where the E_b is defined as $\Delta E_b = E_A - E_0 - E_m$, in which E_A, E_0, and E_m denote the energies of the optimized adsorbed slabs, the corresponding separated slab without the adsorbed cations, and the cations, respectively. As a result, the E_b values increase in the order of **PDMAI$_2$** (49.65 kcal mol^{-1}) < **TDMAI$_2$** (53.62 kcal mol^{-1}) < **PFPDMAI$_2$** (64.53 kcal mol^{-1}) < **PHMAI$_6$** (77.56 kcal mol^{-1}), consistent with the order of surface geometry relaxation. The introduction of surface cations generally will passivate the surface trap states of perovskite films. A surface scanning electron microscope (SEM) was employed to observe the surface morphology influenced by the additional cation modification (Fig. S1†), and the results indicate that introduction of each cation onto the surface will make the perovskite surface grains more dense, which may be attributed to the surface secondary growth of the perovskite. X-ray diffraction (XRD) was further employed to study the crystal structure after the surface secondary reaction (Fig. S2†). The results show that the crystallinities of **PFPDMAI$_2$** and **PHDMAI$_6$** based samples are better than those of others, implying the possibility of better performance of PSCs.

Next, PSC devices were fabricated with a typical stack consisting of fluorine-doped tin oxide (FTO)/TiO_2/SnO_2/perovskite/passivating agent/spiro-OMeTAD/Au to study the passivation effect of synthesized cations. Isopropanol solutions of cations were spin-coated onto the perovskite layer to form a thin organic halide salt layer instead of a 2D perovskite on top of the 3D perovskite surface, expecting to avoid the energy disorder and the efficiency loss at elevated operating temperatures. Fig. 2a represents the illustration of the device structure through cross-section SEM. It is evident that the thickness of the perovskite film is about 600 nm, and it is only one grain thick due to the large gain size of the perovskite, which is favorable to achieve efficient PSCs. We also obtained the cross-section SEM images of **PFPDMAI$_2$** treated perovskite films, which show that a very thin layer is formed on the top of the perovskite, which would protect the perovskite film and result in surface passivation (Fig. 2a).

Current density (J)–voltage (V) characteristics with negligible hysteresis of the devices based on **PFPDMAI$_2$** are compared in Fig. 2c and the J–V curves for the different cations are shown in Fig. 2b with detailed parameters listed in Table 1. Interestingly, all devices having passivating agents show higher PCEs compared to the control devices, in particular with higher V_{oc} and improved FF, under the optimized cation concentration of 4 mg mL^{-1} (Fig. S3 and Table S2†). The effective passivation may be attributed to the high adsorption density on the perovskite, strong adsorption energy of the *ortho*-methylammonium units, and the improved electrostatic interactions with the perovskite defects.

Among the four cations, **PFPDMAI$_2$** showed the maximized passivation effect, boosting the PCE from 21.99% of the control device to 24.02% with a V_{oc} of 1.155 V, a J_{sc} of 24.99 mA cm^{-2}, and a FF of 0.833. The improvement using the fluorinated cation is mostly due to the enhanced V_{oc} and FF, which may be ascribed to the decreased defect densities and reduced non-radiative recombination loss, suggesting that the fluorinated passivation layer serves as a blocking layer impeding iodide migration across the interface. The reproducibility of the devices based on the reference and **PFPMAI$_2$** indicated that both types of PSCs exhibit good reproducibility (Fig. S4†). The integrated J_{sc} values from the IPCE spectra in Fig. 2d match the J–V curve-extracted values (<1% discrepancy). A stabilized power output of 23.95% is shown in Fig. 2e compared to 21.90% of the control device. In addition, the $MAPbI_3$ and $Cs_{0.05}(FA_{0.85}MA_{0.15})_{0.95}Pb(I_{0.85}Br_{0.15})_3$ types of perovskite were also further measured with the **PFPDMAI$_2$** passivation. All the devices with the **PFPDMAI$_2$** treatment exhibit better efficiency, however, all of the PCEs are lower than that of the $FAMAPbI_3$ based composition (Fig. S6, Tables S6 and S7†).

Time-resolved photoluminescence (TRPL) measurements (Fig. 2f) were performed on the FTO/perovskite and FTO/perovskite/**PFPDMAI$_2$** films. TRPL decay time was fitted by a bi-exponential model with the fast (τ_1) and slow (τ_2) components, which indicate the interfacial transportation and recombination. The average delay time (τ_{ave}) is calculated by $\tau_{ave} = \sum A_i\tau_i^2 / \sum A_i\tau_i$, where A_i and τ_i represent the decay amplitude and components of delay time, respectively (Table S3†). For the interfacial recombination, the slow (τ_2) component was considered. When the bare perovskite film was employed for the film, the decay time was 177.7 ns with an average decay time of 139.3 ns. By contrast, a slower decay time with $\tau_2 = 321.7$ ns and an average decay time $\tau = 272.3$ ns were attained for the **PFPDMAI$_2$** based devices. Steady-state fluorescence spectroscopy (PL) was further employed to study the interface recombination of carriers (Fig. 2g). Similarly, the PL also shows a higher lifetime of carriers for the **PFPDMAI$_2$** based sample. Interestingly, when the **PFPDMAI$_2$** was spin-coated on the perovskite film, the peak of PL shifts about 3 nm, which further indicated the passivation of the perovskite film and agrees well with the increased performance of PSCs by the introduction of the cation. The DFT was further employed to study the trap state changes after the **PFPDMAI$_2$** cation interacted with the PbI_3^- anti-defects of the perovskite surface. The results show that the **PFPDMAI$_2$** interfaced with the center of the octahedron, and electrostatically interacted with the PbI_3^- anti-defects (Fig. S7a†). The density of states (DOS) results show that the PbI_3^- anti-defects of the perovskite exhibit trap states within the band gap of the perovskite (Fig. S7b†). However, the gap state is eliminated after the interaction of **PFPDMAI$_2$**. These results further certify that the **PFPDMAI$_2$** cation passivates the trap states of the perovskite, consistent with the TRPL and PL results.

Next, ultraviolet photoelectron spectroscopy (UPS) has been used to explore the energy level change by the passivation of **PFPDMAI$_2$** (Fig. S8†). The results show that employing **PFPDMAI$_2$** increases the valence band (VB) of the perovskite from −5.42 to −5.39 eV (21.22 eV − E_{cutoff} + E_{onset}), which is better matching with the energy of spiro-OMeTAD (−5.2 eV) and facilitates the interface carrier transportation.

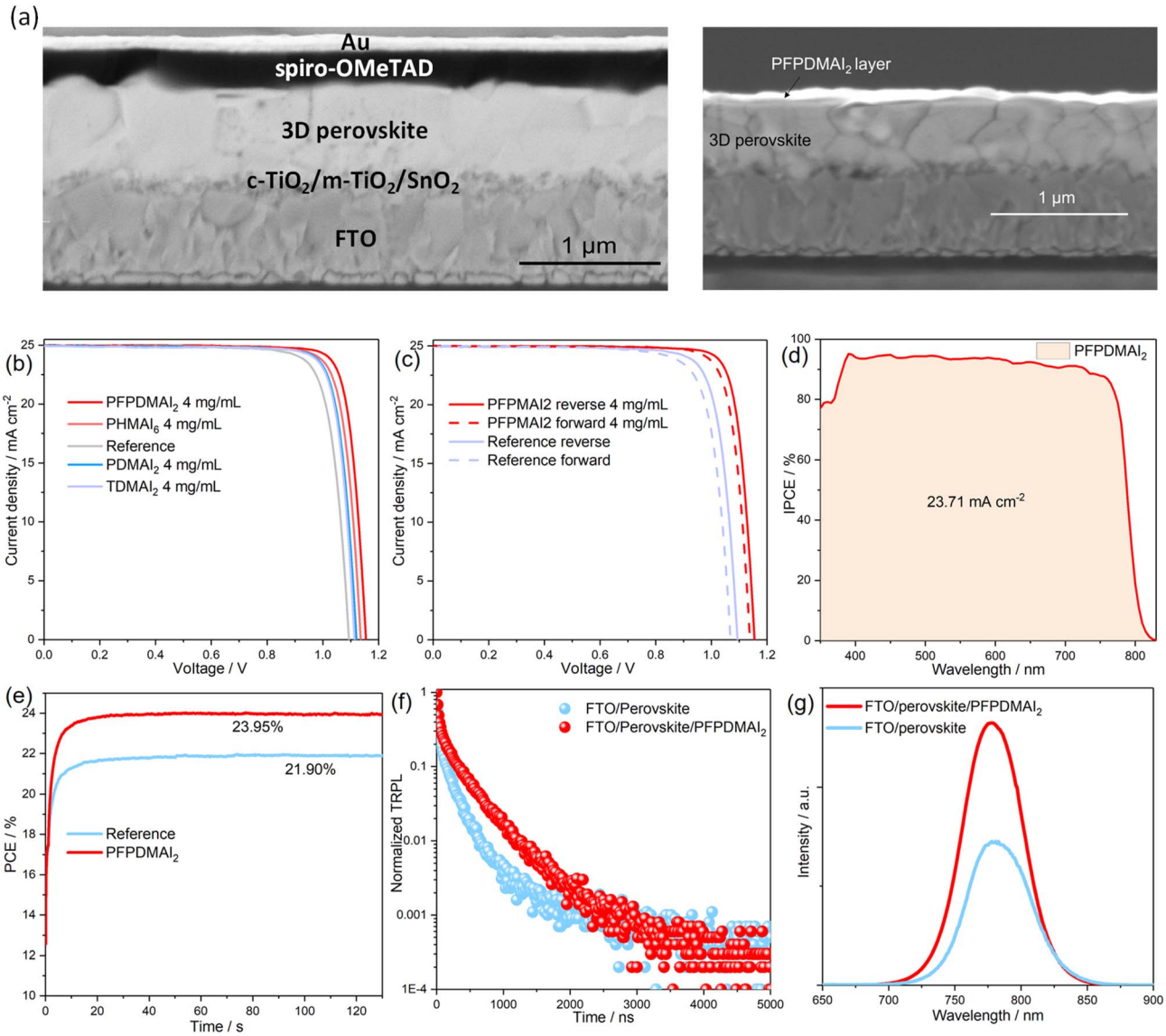

Fig. 2 (a) Cross-sectional SEM of the PSC device (left) and perovskite film treated with the **PFPDMAI$_2$** passivation layer (right); (b) *J*–*V* characteristics of the devices with different passivating agents; (c) *J*–*V* characteristics of the champion devices with or without the **PFPDMAI$_2$** layer measured in both reverse (solid) and forward (dash) scanning directions; (d) IPCE spectrum of the best-performing **PFPDMAI$_2$**-passivated device; (e) stabilized power output for a device with and without **PFPDMAI$_2$**; (f) time-resolved photoluminescence (TRPL) of the perovskite thin films with or without the **PFPDMAI$_2$** layer; (g) PL of the perovskite thin films with or without the **PFPDMAI$_2$** layer.

Table 1 The detailed photovoltaic parameters of PSCs without or with passivating cations under the optimized 4 mg mL^{-1} concentration

Device	J_{sc} [mA cm^{-2}]	V_{oc} [V]	FF/%	PCE [%]
Reference	24.93	1.093	80.7	21.99
PHMAI$_6$	24.96	1.135	82.5	23.37
PDMAI$_2$	24.94	1.121	81.7	22.84
TDMAI$_2$	24.93	1.114	82.2	22.82
PFPDMAI$_2$	24.99	1.154	83.3	24.02

Femtosecond transient absorption spectroscopy (fs-TA) was employed to study the charge transport at the interface. Fig. S9a and b† show the typical ΔOD at various delay times from 50 to 1500 ps. The positive excited-state absorption (ESA) band is present before 720 nm and the negative ground state bleaching (GSB) band is at ~760 nm, which is related to the fluorescent emission from the perovskite. Comparison of the GSB peak at ~767 nm reveals that the negative peak intensity of **PFPDMAI$_2$** is largely decreased due to the faster transportation of the holes. The time evolution profiles of the ESA peak at 767 nm are shown in Fig. S9c.† The ultrafast time below 1000 ps indicates the charge transportation, however, the time scale of 1 ns to 1 μs may be ascribed to the excited-state delay time or recombination dynamics of the perovskite.[51] Thus, the fast component τ_1 was considered to affirm charge transportation for glass/perovskite/spiro-OMeTAD and glass/perovskite/**PFPDMAI$_2$**/spiro-OMeTAD samples. When **PFPDMAI$_2$** is introduced onto

the perovskite surface, the decay times of GSB peaks are dramatically reduced from 805.2 ps to 74.5 ps, which indicated that employing a passivation layer will enhance the interface carrier transportation.

In addition to the improved PCE, the long-term stability was also evaluated to study the influence of different passivation layers on device stability. The light-soaking performance of the unencapsulated PSCs was evaluated by MPPT under 1 sun illumination and an inert atmosphere as shown in Fig. 3a. In general, all passivated devices show significantly improved stability compared with the control device having no post-treatment that degrades to ~70% of the initial PCE. The device passivated with fluorinated **PFPDMAI$_2$** exhibits the highest light stability, maintaining ~94% of its original PCE after 1500 h, outperforming other devices based on **PHMAI$_6$** (90%), **TDMAI$_2$** (~88%), and **PDMAI$_2$** (~86%), respectively, and representing another important advantage of a newly synthesized fluorinated cation. Fig. 3b shows the T_{80} of the stability of the devices. It can be seen that the device with the **PFPDMAI$_2$** cation exhibits a slower decay of efficiency with the T_{80} over 1000 h, whereas the control device reaches the T_{80} line in only 200 h. Next, the PCEs of the unencapsulated devices with and without **PFPDMAI$_2$** under a RH of 10–20% were tracked over time (Fig. 3c). The control device maintained ~79% of the initial PCE after 60 days, compared to that of ~92% for the **PFPDMAI$_2$** passivated device. The water contact angles of the perovskite and the perovskite/**PFPDMAI$_2$** films were employed to realize the reason of stability enhancement (Fig. 3d). The results show that the contact angle increased from 58° to 67° after the treatment with the **PFPDMAI$_2$** salt. The more hydrophobic fluorinated **PFPDMAI$_2$** passivation layer is presumably responsible for reducing moisture penetration and suppressed phase degradation benefiting from the passivation effect.

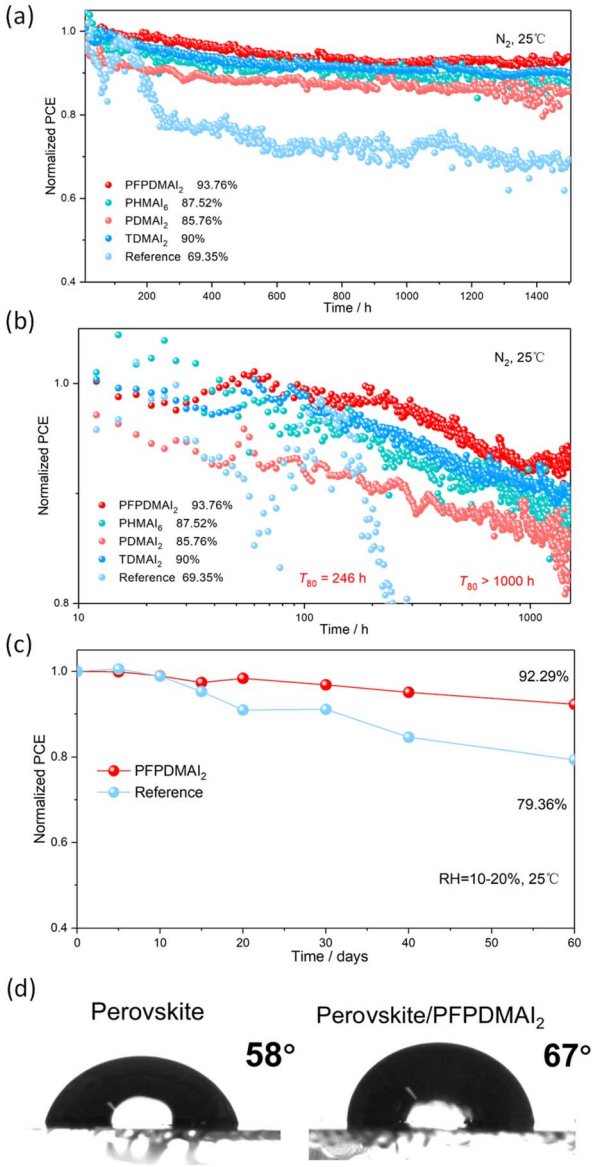

Fig. 3 (a) Maximum power point tracking (MPPT) for 1500 h of the unencapsulated devices under continuous light (100 mW cm^{-2}) illumination at 25 °C in a nitrogen atmosphere; (b) the T_{80} stability of PSCs from (a); (c) evolution of the PCEs for the unencapsulated devices exposed to a controlled relative humidity (RH) of 10–20% in the dark at 25 °C; (d) water contact angles of the perovskite and perovskite/**PFPDMAI$_2$** films.

To conclude, we demonstrate the synthesis and a thorough study of sterically hindered *ortho*-methylammonium cations that are used as passivating agents to form a thin organic halide salt layer in perovskite solar cells (PSCs) instead of forming a 2D perovskite. The impact of different molecularly engineered functional units was revealed by employing optical, photophysical, and photovoltaic measurements. We found that the incorporation of fluorine atoms is beneficial for improved carrier transportation and enhanced device stability due to the passivation of defective perovskite states. The most efficient perovskite devices contained **PFPDMAI$_2$** salt, reaching a PCE of over 24% and excellent long-term stability over 1500 h. The study shows that a simple post-treatment strategy using sterically hindered cations with extra functionality leads to significantly improved PSC efficiency and stability.

Conflicts of interest

There are no conflicts to declare.

Acknowledgements

Financial support from the Research Council of Lithuania *via* grant no. S-MIP-20-20 is greatly acknowledged.

References

1 H. Min, D. Y. Lee, J. Kim, G. Kim, K. S. Lee, J. Kim, M. J. Paik, Y. K. Kim, K. S. Kim, M. G. Kim, T. J. Shin and S. I. Seok, *Nature*, 2021, **598**, 444–450.
2 J. Burschka, N. Pellet, S. J. Moon, R. Humphry-Baker, P. Gao, M. K. Nazeeruddin and M. Grätzel, *Nature*, 2013, **499**, 316–319.
3 N. J. Jeon, J. H. Noh, W. S. Yang, Y. C. Kim, S. Ryu, J. Seo and S. I. Seok, *Nature*, 2015, **517**, 476–480.

4 M. M. Lee, J. Teuscher, T. Miyasaka, T. N. Murakami and H. J. Snaith, *Science*, 2012, **338**, 643–647.
5 C. Wehrenfennig, G. E. Eperon, M. B. Johnston, H. J. Snaith and L. M. Herz, *Adv. Mater.*, 2014, **26**, 1584–1589.
6 M. Saliba, T. Matsui, J. Y. Seo, K. Domanski, J. P. Correa-Baena, M. K. Nazeeruddin, S. M. Zakeeruddin, W. Tress, A. Abate, A. Hagfeldt and M. Grätzel, *Energy Environ. Sci.*, 2016, **9**, 1989–1997.
7 M. A. Green, A. Ho-Baillie and H. J. Snaith, *Nat. Photonics*, 2014, **8**, 506–514.
8 B. Chen, Z. J. Yu, S. Manzoor, S. Wang, W. Weigand, Z. Yu, G. Yang, Z. Ni, X. Dai, Z. C. Holman and J. Huang, *Joule*, 2020, **4**, 850–864.
9 W. S. Yang, B. W. Park, E. H. Jung, N. J. Jeon, Y. C. Kim, D. U. Lee, S. S. Shin, J. Seo, E. K. Kim, J. H. Noh and S. I. Seok, *Science*, 2017, **356**, 1376–1379.
10 W. W. Liu, T. H. Wu, M. C. Liu, W. J. Niu and Y. L. Chueh, *Adv. Mater. Interfaces*, 2019, **6**, 1801758.
11 D. H. Kim, J. B. Whitaker, Z. Li, M. F. A. M. van Hest and K. Zhu, *Joule*, 2018, **2**, 1437–1451.
12 L. Qiu, L. K. Ono and Y. Qi, *Mater. Today Energy*, 2018, **7**, 169–189.
13 Y. Rong, Y. Hu, A. Mei, H. Tan, M. I. Saidaminov, S. I. Seok, M. D. McGehee, E. H. Sargent and H. Han, *Science*, 2018, **361**, eaat8235.
14 K. Rakstys, C. Igci and M. K. Nazeeruddin, *Chem. Sci.*, 2019, **10**, 6748–6769.
15 C. Liu, Y. Yang, K. Rakstys, A. Mahata, M. Franckevicius, E. Mosconi, R. Skackauskaite, B. Ding, K. G. Brooks, O. J. Usiobo, J. N. Audinot, H. Kanda, S. Driukas, G. Kavaliauskaite, V. Gulbinas, M. Dessimoz, V. Getautis, F. De Angelis, Y. Ding, S. Dai, P. J. Dyson and M. K. Nazeeruddin, *Nat. Commun.*, 2021, **12**, 1–9.
16 A. R. B. M. Yusoff, M. Vasilopoulou, D. G. Georgiadou, L. C. Palilis, A. Abate and M. K. Nazeeruddin, *Energy Environ. Sci.*, 2021, **14**, 2906–2953.
17 A. Mahapatra, D. Prochowicz, M. M. Tavakoli, S. Trivedi, P. Kumar and P. Yadav, *J. Mater. Chem. A*, 2020, **8**, 27–54.
18 X. Liu, Z. Yu, T. Wang, K. L. Chiu, F. Lin, H. Gong, L. Ding and Y. Cheng, *Adv. Energy Mater.*, 2020, **10**, 2001958.
19 Y. Cai, J. Cui, M. Chen, M. Zhang, Y. Han, F. Qian, H. Zhao, S. Yang, Z. Yang, H. Bian, T. Wang, K. Guo, M. Cai, S. Dai, Z. Liu and S. Liu, *Adv. Funct. Mater.*, 2021, **31**, 2005776.
20 G. Sathiyan, A. A. Syed, C. Chen, C. Wu, L. Tao, X. Ding, Y. Miao, G. Li, M. Cheng and L. Ding, *Nano Energy*, 2020, **72**, 104673.
21 F. Li, X. Deng, F. Qi, Z. Li, D. Liu, D. Shen, M. Qin, S. Wu, F. Lin, S. H. Jang, J. Zhang, X. Lu, D. Lei, C. S. Lee, Z. Zhu and A. K. Y. Jen, *J. Am. Chem. Soc.*, 2020, **142**, 20134–20142.
22 C. C. Boyd, R. Cheacharoen, T. Leijtens and M. D. McGehee, *Chem. Rev.*, 2019, **119**, 3418–3451.
23 S. G. Motti, D. Meggiolaro, S. Martani, R. Sorrentino, A. J. Barker, F. De Angelis and A. Petrozza, *Adv. Mater.*, 2019, **31**, 1901183.
24 E. Aydin, M. De Bastiani and S. De Wolf, *Adv. Mater.*, 2019, **31**, 1900428.
25 C. M. Wolff, P. Caprioglio, M. Stolterfoht and D. Neher, *Adv. Mater.*, 2019, **31**, 1902762.
26 S. Daskeviciute-Geguziene, Y. Zhang, K. Rakstys, C. Xiao, J. Xia, Z. Qiu, M. Daskeviciene, T. Paskevicius, V. Jankauskas, A. M. Asiri, V. Getautis and M. K. Nazeeruddin, *Adv. Funct. Mater.*, 2022, **33**, 2208317.
27 X. Wang, K. Rakstys, K. Jack, H. Jin, J. Lai, H. Li, C. S. K. Ranasinghe, J. Saghaei, G. Zhang, P. L. Burn, I. R. Gentle and P. E. Shaw, *Nat. Commun.*, 2021, **12**, 1–10.
28 G. Grancini, C. Roldán-Carmona, I. Zimmermann, E. Mosconi, X. Lee, D. Martineau, S. Narbey, F. Oswald, F. De Angelis, M. Graetzel and M. K. Nazeeruddin, *Nat. Commun.*, 2017, **8**, 15684.
29 Q. Zhou, Q. Xiong, Z. Zhang, J. Hu, F. Lin, L. Liang, T. Wu, X. Wang, J. Wu, B. Zhang and P. Gao, *Sol. RRL*, 2020, **4**, 2000107.
30 G. Liu, X. X. Xu, S. Xu, L. Zhang, H. Xu, L. Zhu, X. Zhang, H. Zheng and X. Pan, *J. Mater. Chem. A*, 2020, **8**, 5900–5906.
31 T. Zhao, C. C. Chueh, Q. Chen, A. Rajagopal and A. K. Y. Jen, *ACS Energy Lett.*, 2016, **1**, 757–763.
32 M. A. Mahmud, T. Duong, J. Peng, Y. Wu, H. Shen, D. Walter, H. T. Nguyen, N. Mozaffari, G. D. Tabi, K. R. Catchpole, K. J. Weber and T. P. White, *Adv. Funct. Mater.*, 2022, **32**, 2009164.
33 A. Rajagopal, K. Yao and A. K. Y. Jen, *Adv. Mater.*, 2018, **30**, 1800455.
34 L. Liang, H. Luo, J. Hu, H. Li and P. Gao, *Adv. Energy Mater.*, 2020, **10**, 2000197.
35 Y. Yang, C. Liu, A. Mahata, M. Li, C. Roldán-Carmona, Y. Ding, Z. Arain, W. Xu, Y. Yang, P. A. Schouwink, A. Züttel, F. De Angelis, S. Dai and M. K. Nazeeruddin, *Energy Environ. Sci.*, 2020, **13**, 3093–3101.
36 H. Pan, X. Zhao, X. Gong, Y. Shen and M. Wang, *J. Phys. Chem. Lett.*, 2019, **10**, 1813–1819.
37 F. Ansari, E. Shirzadi, M. Salavati-Niasari, T. Lagrange, K. Nonomura, J. H. Yum, K. Sivula, S. M. Zakeeruddin, M. K. Nazeeruddin, M. Grätzel, P. J. Dyson and A. Hagfeldt, *J. Am. Chem. Soc.*, 2020, **142**, 11428–11433.
38 B. Wang, H. Wang, G. Sathiyan, C. Chen, Y. Xu and M. Cheng, *ACS Appl. Energy Mater.*, 2022, **5**, 5901–5908.
39 C. Igci, H. Kanda, S. M. Yoo, A. A. Sutanto, O. A. Syzgantseva, M. A. Syzgantseva, V. Jankauskas, K. Rakstys, M. Mensi, H. Kim, A. M. Asiri and M. K. Nazeeruddin, *Sol. RRL*, 2022, **6**, 2100667.
40 K. Rakstys, J. Solovjova, T. Malinauskas, I. Bruder, R. Send, A. Sackus, R. Sens and V. Getautis, *Dyes Pigm.*, 2014, **104**, 211–219.
41 Y. Wang, Q. Chen, J. Fu, Z. Liu, Z. Sun, S. Zhang, Y. Zhu, X. Jia, J. Zhang, N. Yuan, Y. Zhou, B. Song and Y. Li, *Chem. Eng. J.*, 2022, **433**, 133265.
42 Y. Li, F. Wu, M. Han, Z. Li, L. Zhu and Z. Li, *ACS Energy Lett.*, 2021, **6**, 869–876.
43 H. Lu, J. Xu, X. Liu, F. Wu and L. Zhu, *Mater. Today Energy*, 2021, **21**, 100780.
44 J. Yuan, Y. Chen, X. Liu and S. Xue, *ACS Appl. Energy Mater.*, 2021, **4**, 5756–5766.

45 Y. Sun, C. Zhao, J. Zhang, Y. Peng, R. Ghadari, L. Hu and F. Kong, *Synth. Met.*, 2022, **285**, 117027.
46 Y. Wang, Q. Liao, J. Chen, W. Huang, X. Zhuang, Y. Tang, B. Li, X. Yao, X. Feng, X. Zhang, M. Su, Z. He, T. J. Marks, A. Facchetti and X. Guo, *J. Am. Chem. Soc.*, 2020, **142**, 16632–16643.
47 C. Igci, S. Paek, K. Rakstys, H. Kanda, N. Shibayama, V. Jankauskas, C. Roldán-Carmona, H. Kim, A. M. Asiri and M. K. Nazeeruddin, *Sol. RRL*, 2020, **4**, 2000173.
48 C. Liu, C. Igci, Y. Yang, O. A. Syzgantseva, M. A. Syzgantseva, K. Rakstys, H. Kanda, N. Shibayama, B. Ding, X. Zhang, V. Jankauskas, Y. Ding, S. Dai, P. J. Dyson and M. K. Nazeeruddin, *Angew. Chem., Int. Ed.*, 2021, **60**, 20489–20497.
49 K. Rakstys, S. Paek, P. Gao, P. Gratia, T. Marszalek, G. Grancini, K. T. Cho, K. Genevicius, V. Jankauskas, W. Pisula and M. K. Nazeeruddin, *J. Mater. Chem. A*, 2017, **5**, 7811–7815.
50 B. Chen, P. N. Rudd, S. Yang, Y. Yuan and J. Huang, *Chem. Soc. Rev.*, 2019, **48**, 3842–3867.
51 J. Xia, P. Luizys, M. Daskeviciene, C. Xiao, K. Kantminiene, V. Jankauskas, K. Rakstys, G. Kreiza, X. X. Gao, H. Kanda, K. G. Brooks, I. R. Alwani, Q. U. Ain, J. Zou, G. Shao, R. Hu, Z. Qiu, A. Slonopas, A. M. Asiri, Y. Zhang, P. J. Dyson, V. Getautis and M. K. Nazeeruddin, *Adv. Mater.*, 2023, **35**, 2300720.

